Microporous and Mesoporous Materials 181 (2013) 146–153

Contents lists available at ScienceDirect

Microporous and Mesoporous Materials

journal homepage: www.elsevier.com/locate/micromeso

Porous TiO_2 nanowires derived from nanotubes: Synthesis, characterzation and their enhanced photocatalytic properties

Zhen Jin, Fan-Li Meng, Yong Jia, Tao Luo, Jin-Yun Liu, Bai Sun, Jin Wang, Jin-Huai Liu, Xing-Jiu Huang *

Research Center for Biomimetic Functional Materials and Sensing Devices, Institute of Intelligent Machines, Chinese Academy of Sciences, Hefei 230031, China

ARTICLE INFO

Article history:
Received 6 May 2013
Received in revised form 4 July 2013
Accepted 4 July 2013
Available online 15 July 2013

Keywords:
TiO_2
Porous nanowires
Structure transformation
Dissolution–recrystallization
Photocatalytic activity

ABSTRACT

Anatase porous TiO_2 nanowires were synthesized *via* simple *in situ* hydrothermal treatment of the amorphous anodic TiO_2 nanotubes in urea aqueous solution at 70 °C. The morphology transformation process was also analyzed so that hydroxide induced dissolution–recrystallization mechanism was proposed. Due to the coarse surface and porous structure, the porous TiO_2 nanowires possess a large surface area of 267.56 $m^2 g^{-1}$, which is almost 4 times higher than that of amorphous anodic TiO_2 nanotubes. The photocatalytic properties of the porous TiO_2 nanowires towards MB, phenol and Rhodamine 6G were investigated. The porous TiO_2 nanowires display better photocatalytic activity than that of TiO_2 nanotubes or Degussa P25. The enhanced photocatalytic activity is attributed to the porous structure and the large specific surface area. Such porous TiO_2 nanowires maybe considered as an ideal photocatalyst for the rapid photodegradation of organic pollutant in water. Furthermore, this facile, low-cost and environmentally friendly method is highly expected to innovate the design and fabrication of highly photoactive porous TiO_2 nanowires, which have potential applications in photocatalysis and solar energy conversion.

1. Introduction

Titanium dioxide (TiO_2), as one of the most commonly used semiconductor materials, has attracted a lot of attention due to its unique photoinduced activity explored for applications in photocatalysis [1–3], environmental pollution control [4–7], and solar energy conversion [8,9]. Due to these reactions usually taking place on the surface of TiO_2, the properties are strongly related to the surface area and local microstructures [10,11]. Therefore, nanoscaled TiO_2 with large surface area and specific morphology have attracted great attention [12,13]. Up to today, many methods, such as anodization [14], template techniques [15], hydrothermal processes [16], and soft chemical processes [17] have been used to synthesize TiO_2 nanomaterials with high photocatalytic activity. Amongst these synthesis strategies, the electrochemical anodization process as a facile, cheap and straightforward method has been widely utilized to large-scaled preparation of TiO_2 nanotubes with controllable size and morphology [18–20]. However, smooth surface, relative low surface area and the amorphous structure of the obtained anodic TiO_2 nanotubes result in low light utilization efficiency and photogenerated charges separation efficiency, thus leading to the poor photocatalytic activity [21,22]. Many efforts have been made to enhance the photocatalytic activity of the anodic TiO_2 nanotubes. For example, annealing of anodic TiO_2 nanotubes in air contributes to converting the amorphous TiO_2 into anatase, which can efficiently enhance the photocatalytic performance [23]. Decorating the anodic TiO_2 nanotubes with the other materials, such as noble metals and other semiconductors, can also improve the photocatalytic performance [24–26]. However, those methods are expensive and high energy consumption. Recently, considerable efforts have been shifted to the architecture of 1D TiO_2 hierarchical nanostructures derived from TiO_2 nanotubes. By adjusting the phase and microstructure of the anodic TiO_2 nanotubes, desired high photocatalytic activity can be achieved. For example, through a derivative anodic method, tube-in-tube TiO_2 nanostructure possessing high surface area were synthesized, which showed enhanced photocatalytic performance [27]. Hierarchical TiO_2 nanotubes were obtained via chemical etching of the anodic TiO_2 nanotubes, exhibiting high photocatalytic activity due to their good crystallinity [28]. Despite the great efforts contributed by many groups, seeking strategies for constructing anodic TiO_2 nanotubes with high surface area and anatase phase has still been an attractive ongoing task.

Herein, we demonstrate the synthesis of porous TiO_2 nanowires composed of anatase TiO_2 nanoparticles at low temperature*via* in situ hydrothermal treatment towards amorphous anodic TiO_2 nanotube arrays. Due to the coarse surface and porous structure, the porous TiO_2 nanowires possess a large surface area of 267.56 $m^2 g^{-1}$, which is almost 4 times higher than that of amorphous anodic TiO_2 nanotubes. The anatase porous structure and large surface area of the porous TiO_2 nanowires lead to great

* Corresponding author. Tel.: +86 551 5591142; fax: +86 551 5592420.
E-mail address: xingjiuhuang@iim.ac.cn (X.-J. Huang).

1387-1811/$ - see front matter © 2013 Published by Elsevier Inc.
http://dx.doi.org/10.1016/j.micromeso.2013.07.006

enhancement of the photodegration of organic pollutants. The photodegration rate of the organic pollutant mehtylene blue (MB) under UV irradiation from the porous TiO_2 nanowires is 4.5 times faster than that from the amorphous TiO_2 nanotubes, and even higher than that from Degussa P25. In addition, the porous TiO_2 nanowires exhibit high photocatalytic activity in degradating phenol and Rhodamine 6G (R6G) as well. This facile, cost-effective and environmentally friendly method is anticipated to innovate the fabrication of highly photoactive porous TiO_2 nanowires, which have potential applications in environment and solar energy conversion.

2. Experimental

All reagents were commercially available from Sinopharm Chemical Reagent Co., Ltd. (China) with analytical grade and were used without further purification. Degussa P25 TiO_2 (80% anatase and 20% rutile) was purchased from Guangzhou Huali Sen Trading Co., Ltd. The average particle size of P25 is 21 nm, and the specific surface area of which is 45.96 $m^2\ g^{-1}$.

The synthesis of the porous TiO_2 nanowires was divided into two steps. Firstly, TiO_2 nanotubes were fabricated by anodizing the pure Ti sheet as described previously [29,30]. In brief, the high-purity (99.999%) titanium plate was anodized in mixing electrolyte of ethylene glycol and ammonium fluoride (0.1 M) for 4 h. The anodizing voltage was 60 V and the temperature of the electrolyte was kept at 20 °C. Subsequently, the sample was rinsed with deionized water. Then, the as-fabricated TiO_2 nanotubes were put into a vessel which contained 0.1 M urea solution (100 ml). After heating at 70 °C for 10 h, white plates were collected from the solution. The as-prepared porous TiO_2 nanowires were washed with deionized water and dried in air.

The anatase TiO_2 nanotubes were synthesized by annealing the as-prepared anodic TiO_2 nanotubes at 500 °C for 2 h.

The morphologies of the samples were examined by field-emission scanning electron microscopy (FE-SEM; FEI Sirion-200) and high resolution transmission electron microscopy (HRTEM; JEM-2010). The crystal structure of the samples was determined by X-ray diffraction (XRD, Philips X'pert PRO) with Cu K_α radiation.

The photocatalytic activities of the various samples were evaluated based upon the removal of stimulated organic pollutants, such as methylene blue (MB), phenol and R6G in the solution. In a typical photocatalytic experiment, 50 ml aqueous solution containing certain amount of stimulated organic pollutants and the as-synthesized product (30 mg) deprived from Ti foil, as catalyst, was maintained in suspension by a magnetic stirrer. A 150 W high pressure mercury lamp with a maximum emission at 365 nm was positioned at about 10 cm above the photo-reactor. Prior to irradiation, the suspension was ultrasonicated for 3 min and magnetically stirred for 1 h in dark to ensure adsorption–desorption equilibration. Then, UV light was turned on. During the given time intervals, 4 ml of solution has been taken from the suspension and centri-

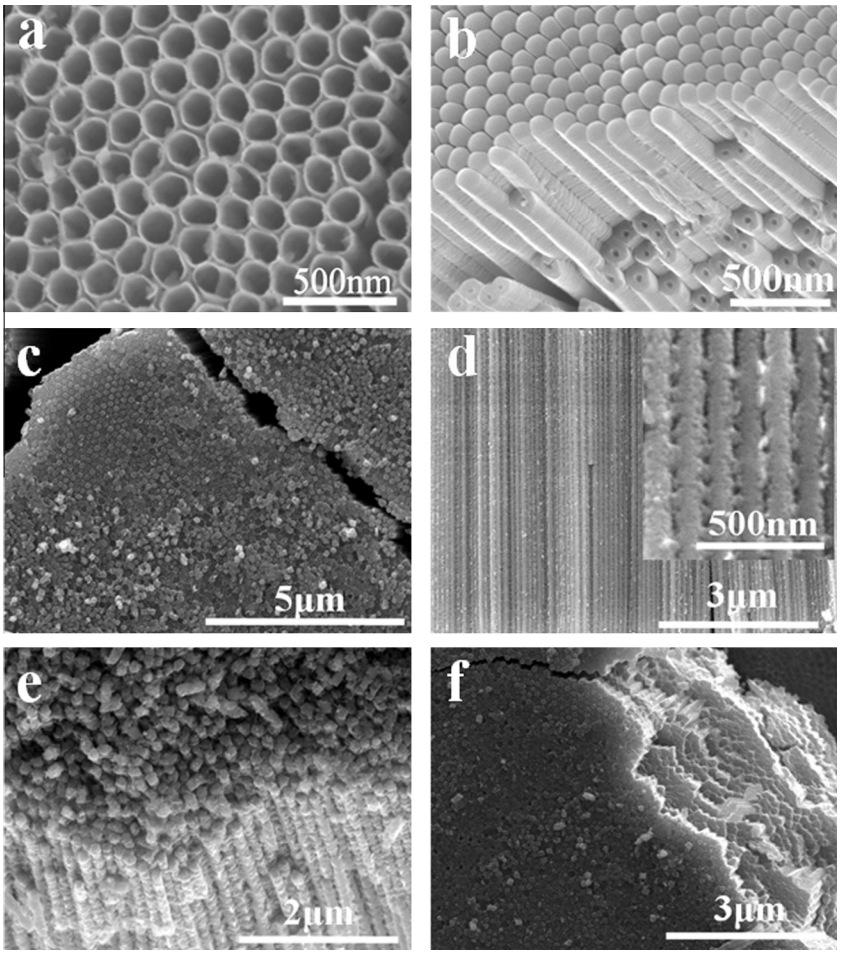

Fig. 1. SEM images of TiO_2 nanotubes and porous TiO_2 nanowires: (a, b) top-view of the anodic TiO_2 nanotubes, (b) cross-section and surface view of the bottom side of the anodic TiO_2 nanotubes, (c) top-view of the porous TiO_2 nanowires, (d) cross-section images of the porous TiO_2 nanowires, the inset is the enlarged image, (e) high and (f) low magnifications cross-section and surface view of the porous TiO_2 nanowires.

fuged at 10,000 rpm for 5 min to remove catalysts. The concentrations of MB, phenol and R6G were monitored by UV–vis spectroscopy (CARY-5E).

3. Results and discussion

3.1. Structure of the Porous TiO_2 nanowires

Fig. 1a and b show the top-view and cross-sectional SEM images of the anodic TiO_2 nanotubes. The open mouth and the closed end of the tubes with ca. 165 nm outer diameters can be clearly observed. Moreover, the inner diameters of the nanotubes at top side are larger than those at bottom side, indicating the taper hollow structure of the nanotubes. If the product is treated via urea, the open mouth can be disappeared, which is shown from the top-view SEM image in Fig. 1c. And urea treatment cause formation of rough surface, as shown in Fig. 1d. The cross-sectional images of treated products in Fig. 1e and f show disappearance of tube-like structure.

TEM was also employed to characterize the samples before and after urea treatment. Fig. 2a shows a typical TEM image of the anodic TiO_2 nanotubes, demonstrating the diameter of 160 nm, which is in agreement with the SEM results. The corresponding selected area electron diffraction pattern (SAED) (the inset of Fig. 2a) indicates the amorphous structure of the anodic TiO_2 nanotubes. TEM images of urea-treated products are shown in Fig. 2b. Surprisingly, it is very clear that the tube-like structure is transformed to the rough porous nanowires after urea treatment. Furthermore, it can be observed that the obtained nanowires are composed of nanoparticles. The SAED pattern shown in inset of Fig. 2b presents series of concentric rings with different radii, indicating their polycrystalline nature of the porous TiO_2 nanowires. HRTEM image shown in Fig. 2c shows that the fringe spacing are 0.47 nm and 0.35 nm, respectively, which match well with those of the lattice space of (0 0 2) and (1 0 1) of anatase TiO_2. Fig. 2d shows the representative EDS spectra of porous nanowires, the molar ratio of Ti:O is 1:1.93, which is very close to the stoichiometry of TiO_2. Fig. 2e is the corresponding XRD pattern of the TiO_2 nanotubes and porous TiO_2 nanowires. As for TiO_2 nanotubes, no diffraction peak was observed, which is in agreement with the SAED result. However, all of the diffraction peaks should be indexed to TiO_2 anatase (JCPDS File 89-4203) after urea-treatment, and the amorphous TiO_2 could be changed to crystalline TiO_2. More importantly, the tube-like structures are turned into anatase porous TiO_2 nanowire. Previous reports indicated that the amorphous anodic TiO_2 nanotubes always need to calcine at about 500 °C in the air so as to achieve anatase polycrystalline. In contrast, the amorphous anodic TiO_2 nanotubes can be conveniently transformed to anatase porous nanowire at the temperature as low as 70 °C in present experiments.

3.2. Structure change mechanism

To study the morphological evolution from TiO_2 nanotubes to porous TiO_2 nanowiers, time-dependent experiments were

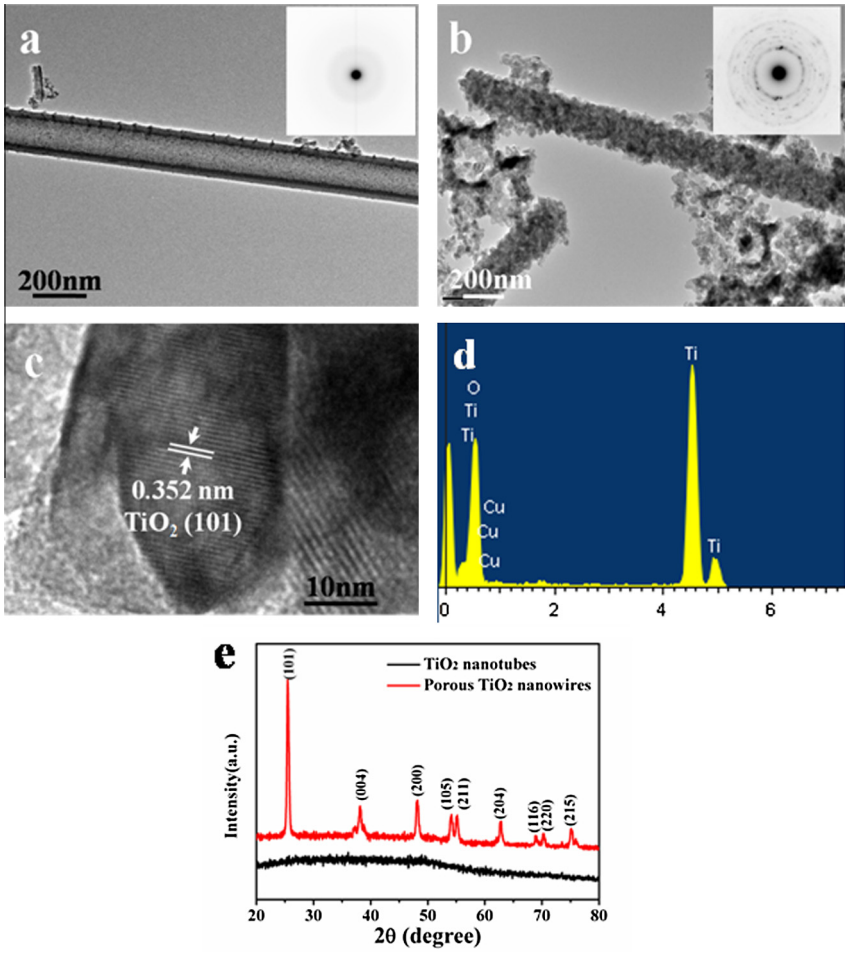

Fig. 2. (a) TEM image of a single TiO_2 nanotube (inset is the corresponding SEAD), (b) TEM image of the porous TiO_2 nanowires (inset is the corresponding SEAD), (c) HRTEM image of the porous TiO_2 nanowires, (d) EDS of the porous TiO_2 nanowires, (e) XRD pattern of the TiO_2 nanotubes and porous nanowires.

performed. Fig. 3 shows the products prepared at different growth stages, i.e., the left, middle and right columns corresponding to the top side, lower part SEM images and TEM images, respectively. Initially, the TiO_2 nanotubes as the precusor were added into urea solution under 70 °C. Fig. 3a presents the morphology of TiO_2 nanotubes, as described before, in which the nanotublar structure and smooth surface wall can be observed clearly. Although the TiO_2 nanotubes remain nanotublar structure after 2 h, the open mouth becomes smaller both at the top side (the left in Fig. 3b) and lower part (the middle in Fig. 3b). As seen from the corresponding TEM image (the right in Fig. 3b), the smooth nanotubes turned to be rough and porous nanotubes, which are composed of nanoparticles. When prolonging the treated time to 4 h, the open mouths of the nanotubes at the top side can still be observed, but the diameter of the open mouths decreases (the left in Fig. 3c); at the lower part, the former opened mouths were closed, indicating the formation of nanowire (the middle in Fig. 3c). Interestingly, the corresponding TEM image (the right in Fig. 3c) shows the combination of the porous nanotube and porous nanowire. Accompany with the reaction time further prolonging to 6 h, it can be found that at both the top side and lower part (the left and middle in Fig. 3d), the open mouths disappear, and the corresponding TEM image (the right in Fig. 3d) also illustrates the nanowire structure.

3.3. Growth mechanism

Based on the above experimental results and analysis, we propose that the morphology evolution of the porous TiO_2 nanowires could be attributable to dissolution–recrystallization process, as shown in Fig. 4. It is well known that TiO_2 is amphoteric oxide [31], besides acid solution [32], it also can slightly dissolve in alkaline solutions [33–35]. In our case, the TiO_2 nanotubes were immersed into urea solution (shown in Fig. 4a). When the solution was heated at 70°C, hydroxyl ions can be generated because of hydrolysis of the urea, resulting in the alkalization of the solution [36]. In heated solutions, the surface atoms of TiO_2 nanotubes would firstly act with hydroxyl ions to form TiO_3^{2-}, as described in Eq. (1). As the dissolution of TiO_2 nanotube walls continues, the OH^- inside the nanotube is consumed faster than that outside of the nanotube, because the OH^- inside the nanotube is difficult to exchange with that outside the nanotubes by the confinement of the nanoscaled hole of the nanotube. When the concentration of

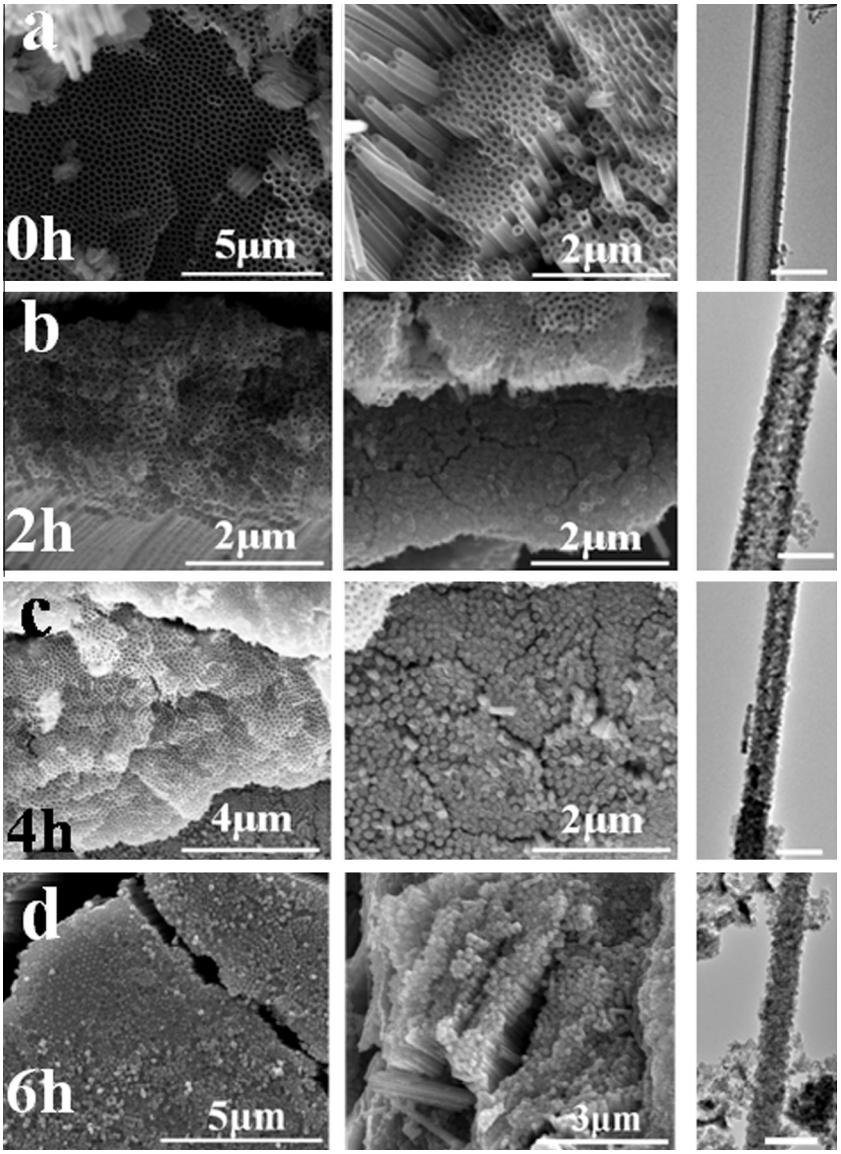

Fig. 3. Morphology transformation from the TiO_2 nanotubes at different reaction times: (a) 0 h; (b) 2 h; (c) 4 h; (d) 6 h. The left and middle columns show the SEM images of the top and lower part, while the third column shows the corresponding TEM images of TiO_2 nanostructures.

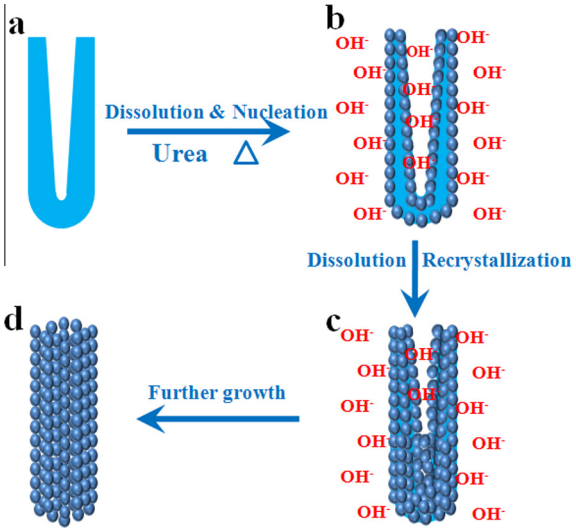

Fig. 4. Schematic illustration of the morphological transformation from the TiO_2 nanotubes to the porous nanowires.

OH^- inside the nanotube decreases to a certain value, TiO_3^{2-} presents a hydrolytic reaction to transform into TiO_2, as shown in Eq. (2). The recrystallized TiO_2 spontaneously nucleates onto the residual nanotube frame, which can provide many high-energy sites for nanocrystallines (shown in Figs. 4b and 3b). As the etching proceeds, more and more TiO_2 nuclei can be formed and grown up within the nanotubes. As the result of the etching of the TiO_2 frames and the formation and growth of TiO_2 nuclei nanocrystallines, the inner space of the nanotube was gradually occupied by TiO_2 nanocrystallines, and the diameter of the nanotube gradually decreased. As described before, the as-prepared TiO_2 nanotubes possess taper hollow structure, thus, the narrow part at the bottom would be fully occupied by TiO_2 nanocrystallines and firstly transformed to porous nanowires while the upper part remain nanotublar morphology (as shown in Figs. 4c and 3c). However, the reaction will not stop in that TiO_2 prefers to nuclei and growth on upper part after bottom part is fully occupied. With the increase of reaction time, the upper part of TiO_2 nanotubes would be full of TiO_2 nanocrystals, and the whole nanotube finally transformed into nanowires composed of TiO_2 nanocrystals (Figs. 4d and 3d).

$$TiO_2 + 2OH^- \rightarrow TiO_3^{2-} + H_2O \quad (1)$$

$$TiO_3^{2-} + H_2O \rightarrow TiO_2 + 2OH^- \quad (2)$$

3.4. N_2 adsorption–desorption analysis

The microstructure of the porous TiO_2 nanowires was further characterized with the N_2 adsorption/desorption isotherms. Fig. 5a and b present the nitrogen adsorption–desorption isotherms and BJH pore size distribution curves of the TiO_2 nanotubes and porous TiO_2 nanowires. Both samples exhibited a type IV isotherm of a type H3 hysteresis loop (according to IUPAC classification [37]), typical of mesoporous materials. The pore size distribution of the TiO_2 nanotubes shows a bi-modal size distribution, with the smaller sizes peaking at 20 nm and the larger sizes at 100 nm. The smaller mesopores can be related to the pores formed between stacked nanotubes, while larger mesopores reflect the hollow structure of the nanotubes. The pore size of the porous TiO_2 nanowires also exhibit two distributions, with the smaller sizes peaking at sub 2 nm and the larger sizes at 20 nm. The larger mesopores can also be related to the pores formed between stacked nanowires, and the smaller mesopores would be attributed to be the stack of nanoparticles within nanowires. The nanoholes within nanotubes are occupied by nanoparticles due to the urea-treatment. As a result, the pore sizes peak of 100 nm within porous TiO_2 nanowires vanishes while the peak of 10 nm appeared, which further confirmed the SEM and TEM results. The BET specific surface area and pore volume of the porous TiO_2 nanowires is determined to be 267.56 $m^2\ g^{-1}$ and 0.31 $cm^3\ g^{-1}$, respectively, which are significantly higher than the values of porous TiO_2 nanowires (70.28 $m^2\ g^{-1}$ and 0.12 $cm^3\ g^{-1}$). Hence, the porous TiO_2 nanowires could be considered as a promising photocatalystic candidate for water treatment thanks to high BET surface area, high value of pore volume and ideal pore size distribution.

3.5. Optical properties

The optical properties of the porous TiO_2 nanowires and TiO_2 nanotubes were investigated by UV–vis diffuse reflectance spectra (Fig. 6). It can be seen that, there is a small peak at 474 nm within the spectrum of the TiO_2 nanotubes, while no peak can be observed to the porous TiO_2 nanowires, indicating the color change from brown to white. Furthermore, compared to TiO_2 nanotubes, the porous TiO_2 nanowires showed the higher UV light absorption. Obviously, the UV–vis absorption would be affected considerably by the morphological changes, and the rough surface and porous structure of the porous TiO_2 nanowires can allow multiple reflections of UV light, which enhances light-harvesting and thus increases the quantity of photogenerated electrons and holes available to participate in the photocatalytic decomposition process [38].

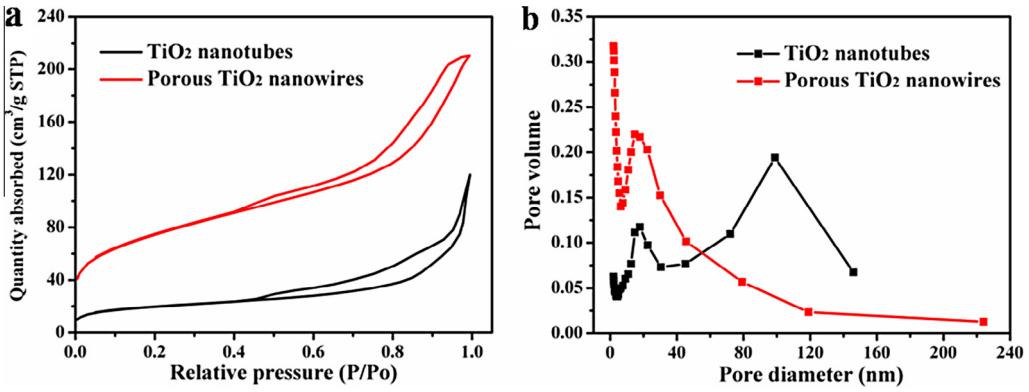

Fig. 5. (a) N_2 adsorption–desorption isotherm of the TiO_2 nanotubes and porous TiO_2 nanowires, and (b) the corresponding pore size distribution.

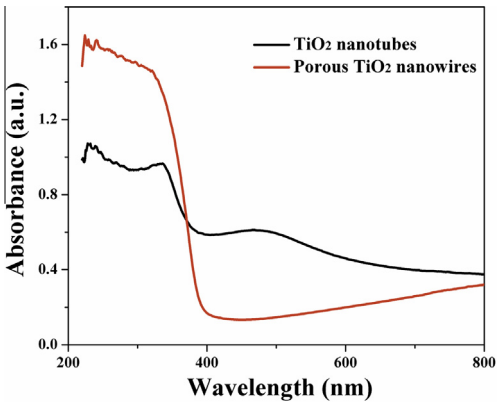

Fig. 6. UV–vis absorption spectrum of the TiO_2 nanotubes and porous TiO_2 nanowires.

3.6. Photocatalytic activity

As far as TiO_2 photocatalyst is concerned, the anatase phase and surface area are the most important criteria.[27,39,40]. High photocatalytic efficiency of the porous TiO_2 nanowires could be expected due to the anatase phase and high surface area within the porous TiO_2 nanowires. In order to demonstrate the functionality of the as-fabricated porous TiO_2 nanowires, their photocatalytic activity was evaluated based on the removal of methylene blue (MB) dye in the aqueous solution. For comparison, the photocatalytic activity of the amorphous TiO_2 nanotubes, anatase TiO_2 nanotubes and P25 particles are also investigated. Fig. 7a displays the variation of the photocatalytic activity of different samples determined at the maximal absorption wavelength of MB (664 nm) with the time of irradiation. As expected, the porous TiO_2 nanowires exhibit superior photocatalytic performance than other photocatalysts. MB is almost completely photodegraded by the porous TiO_2 nanowires within 80 min, while 40%, 75% and 90% of MB are removed by amorphous TiO_2 nanotubes, anatase TiO_2 nanotubes and P25, respectively. As shown in Fig. 7b, the MB photodegration kinetics of various photocatalysts were also investigated. After the natural logarithm of residual phenol concentration vs. UV irradiation time, the linear relationship of $\ln(C_0/C)$ vs time shows that the photoelectrocatalytic degradation of MB follows pseudofirst-order kinetics: $\ln(C_0/C) = kt$, where C_0/C is the normalized MB concentration, t is the reaction time, and k is the apparent reaction rate in min^{-1}. The apparent photodegradation rate constant by the porous TiO_2 nanowires is 0.0426 min^{-1}, which is 4.35 times more than that of amorphous TiO_2 nanotubes (0.0098 min^{-1}), 2.18 times than that of anatase TiO_2 nanotubes (0.0195 min^{-1}) and 1.26 times than that of P25 (0.0337 min^{-1}). Besides MB, phenol and R6G with the concentration of 15 mg l^{-1} were also employed to evaluate the photocatalytic activity of the porous TiO_2 nanowires. From Fig. 8a

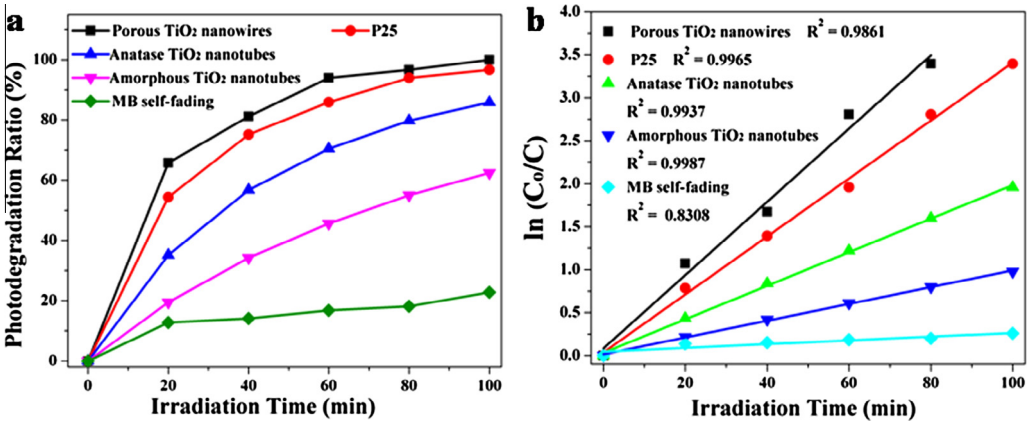

Fig. 7. (a) The variation of photocatalytic degradation ratio of MB over the porous TiO_2 nanowires, amorphous TiO_2 nanotubes, anatase TiO_2 nanotubes, P25 and self-fading, (b) the pseudo first-order kinetic rate plots for the photodegradation of MB.

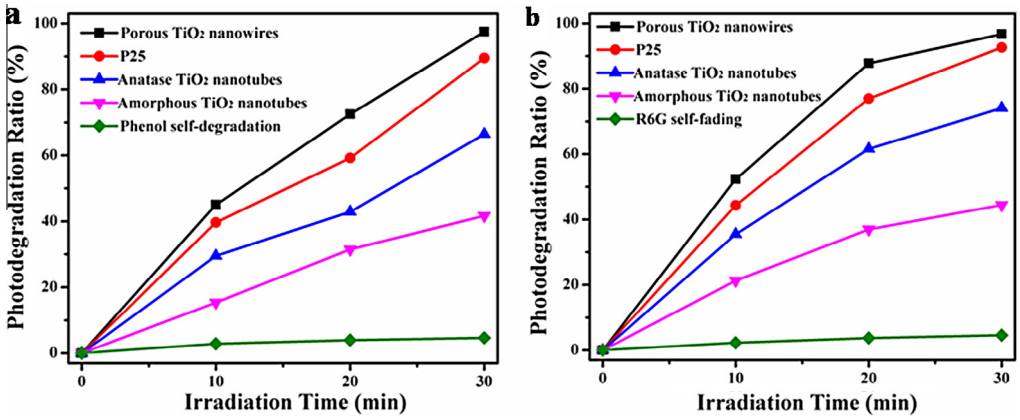

Fig. 8. The variation of photocatalytic degradation of phenol (a) and R6G (b) over the porous TiO_2 nanowires, anatase TiO_2 nanotubes amorphous TiO_2 nanotubes, P25 and self degradation with time of irradiation.

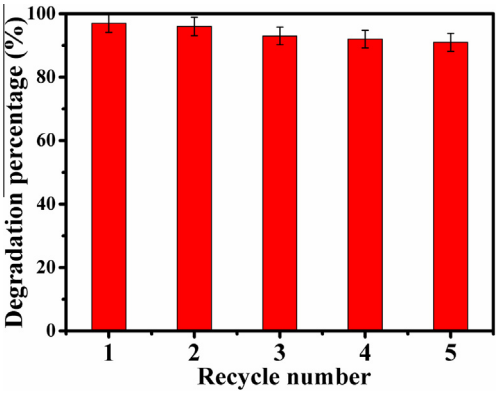

Fig. 9. Cyclic degradation of MB by porous TiO_2 nanowires.

and b, it is clearly that, towards phenol and R6G, the porous TiO_2 nanowires also exhibit higher photocatalytic performance than other samples. Both of phenol and R6G can be completely photodegraded by the porous TiO_2 nanowires within 30 min. Such dramatic enhancement of catalytic activity can be attributed to the synergistic effects of morphology and structure transformation. Firstly, the anatase structure of porous TiO_2 nanowires would facilitate electron transfer from bulk to surface, and thus inhibit their recombination with photoinduced holes, leading to higher quantum efficiency. Meanwhile, the porous TiO_2 nanowires possess much higher BET surface area than TiO_2 nanotubes, and the increase of the surface area can provide more active catalytic sites. Furthermore, the porous structured of TiO_2 nanowires with smaller textural mesopores and larger pore volume would provide reactant substances of different size transport circumstances as compared to those in open medium, and expedite mass transportation. In addition, the compact stacked nanoparticles within porous TiO_2 nanowires can allow multiple reflections of UV light, which enhances light-harvesting and thus increases the quantity of photogenerated electrons and holes available to participate in the photocatalytic degradation of organic pollutions. These factors are beneficial to form more surface hydroxyl radicals to enhance the photocatalytic degradation of phenol. Additionally, based on the well-known fact that anatase phase TiO_2 possesses higher photocatalytic activity than amorphous TiO_2, the anatase phase characteristics of the present porous TiO_2 nanowires after urea-treatment exhibits superior photocatalytic behaviors. Therefore, it can be concluded that porous TiO_2 nanowires can be acted as excellent photocatalysts.

The renewable potocatalytic activity has to be investigated in that the reuse performance is also a key role for the applications of photocatalytic materials. The result is presented in the same manner as shown in Fig. 9, from which we can see that the photocatalytic activity of the porous TiO_2 nanowires is very stable. Even if after 5 cycles under UV irradiation, more than 90% of MB was degradated within 80 min, indicating that the porous TiO_2 nanowires is stable and effective for the removal of organic pollutants in water. Obviously, the porous TiO_2 nanowire prepared in our experiments is a promising photocatalyst due to its excellent activity and good recycle performance.

4. Conclusions

In conclusion, anatase porous TiO_2 nanowires have been produced spontaneously from anodized amorphous TiO_2 nanotubes in urea solution at a temperature as low as 70 °C. The phase and morphology transformation process of the TiO_2 nanotubes are characterized and a mechanism of hydroxide induced dissolution and recrystallization is proposed. Due to the hydrolysis of urea, the amorphous TiO_2 nanotube walls can be gradually etched by hydroxyl ions and dissolved. When the concentration of OH^- inside the nanotubes decreases to a threshold value, the dissolved TiO_2 can recrystalline from solution, and nucleate onto the residual nanotube frame and grow up within the nanotubes. During the dissolve–recrystalline process, more and more TiO_2 nuclei has been formed and grown up within the nanotubes, finally fulfilled the inner space of nanotubes for yielding anatase porous TiO_2 nanowires. The surface area of porous TiO_2 nanowires reaches 267.56 $m^2\ g^{-1}$, which is almost 4 times higher than that of TiO_2 nanotubes. The photodegration rate of the organic pollutant mehtylene blue (MB) under UV irradiation by the porous TiO_2 nanowires is 4.35 times higher than that of the TiO_2 nanotubes, and much higher than that of Degussa P25. Besides degradating MB, the porous TiO_2 nanowires also exhibit high photocatalytic activity in degradating phenol and R6G. The enhanced photocatalytic activity achieved from the porous TiO_2 nanowires is ascribed to the porous structure and large surface area. The results demonstrate a facile and practical route for designing and architecting highly photoactive 1D TiO_2-based porous functional materials, which have potential use in photocatalysis and solar energy conversion.

Acknowledgments

This work is supported by the National Basic Research Program of China (2011CB933700) and the National Natural Science Foundation of China (61104205, 61071054, 51002157, 11205204, 21077106 and 21177131). Xing-Jiu Huang also thanks to the financial support from One Hundred Person Project of the Chinese Academy of Sciences, China.

References

[1] T. Tachikawa, S. Yamashita, T. Majima, J. Am. Chem. Soc. 133 (2011) 7197–7204.
[2] Z. Frontistis, V.M. Daskalaki, A. Katsaounis, I. Poulios, D. Mantzavinos, Water Res. 45 (2011) 2996–3004.
[3] B.H. Xu, B.Z. Lin, Q.Q. Wang, X.T. Pian, O. Zhang, L.M. Fu, Micropor. Mesopor. Mater. 147 (2012) 79–85.
[4] L.B. Xiong, F. Yang, L.L. Yan, N.N. Yan, X. Yang, M.Q. Qiu, Y. Yu, J. Phys. Chem. Solids 72 (2011) 1104–1109.
[5] M.R. Prairie, L.R. Evans, B.M. Stange, S.L. Martinez, Environ. Sci. Technol. 27 (1993) 1776–1782.
[6] G. Liu, H.G. Yang, X.W. Wang, L.N. Cheng, H.F. Lu, L.Z. Wang, G.Q. Lu, H.M. Cheng, J. Phys. Chem. C 113 (2009) 21784–21788.
[7] N. Bao, Y.A. Li, Z.T. Wei, G.B. Yin, J.J. Niu, J. Phys. Chem. C 115 (2011) 5708–5719.
[8] H.Q. Wang, M. Miyauchi, Y. Ishikawa, A. Pyatenko, N. Koshizaki, Y. Li, L. Li, X.Y. Li, Y. Bando, D. Golberg, J. Am. Chem. Soc. 133 (2011) 19102–19109.
[9] C.Y. Cho, J.H. Moon, Adv. Mater. 23 (2011) 2971.
[10] G.H. Tian, Y.J. Chen, W. Zhou, K. Pan, C.G. Tian, X.R. Huang, H.G. Fu, CrystEngComm 13 (2011) 2994–3000.
[11] Z.Y. Zhang, F. Zuo, P.Y. Feng, J. Mater. Chem. 20 (2010) 2206–2212.
[12] H.G. Yang, C.H. Sun, S.Z. Qiao, J. Zou, G. Liu, S.C. Smith, H.M. Cheng, G.Q. Lu, Nature 453 (2008) U634–U638.
[13] P. Kubiak, T. Froschl, N. Husing, U. Hormann, U. Kaiser, R. Schiller, C.K. Weiss, K. Landfester, M. Wohlfahrt-Mehrens, Small 7 (2011) 1690–1696.
[14] R. Beranek, H. Kisch, Electrochem. Commun. 9 (2007) 761–766.
[15] Y.T. Cui, J.S. Wang, H.Y. Li, Z.Z. Wang, Chin. J. Inorg. Chem. 25 (2009) 1274–1278.
[16] J.K. Liu, T.C. An, G.Y. Li, N.Z. Bao, G.Y. Sheng, J.M. Fu, Micropor. Mesopor. Mater. 124 (2009) 197–203.
[17] G.J.A.A. Soler-Illia, P.C. Angelome, M.C. Fuertes, D. Grosso, C. Boissiere, Nanoscale 4 (2012) 2549–2566.
[18] H.E. Prakasam, K. Shankar, M. Paulose, O.K. Varghese, C.A. Grimes, J. Phys. Chem. C 111 (2007) 7235–7241.
[19] W. Chanmanee, A. Watcharenwong, C.R. Chenthamarakshan, P. Kajitvichyanukul, N.R. de Tacconi, K. Rajeshwar, J. Am. Chem. Soc. 130 (2008) 965–974.
[20] G.K. Mor, K. Shankar, M. Paulose, O.K. Varghese, C.A. Grimes, Nano Lett. 6 (2006) 215–218.
[21] Y.K. Lai, L. Sun, Y.C. Chen, H.F. Zhuang, C.J. Lin, J.W. Chin, J. Electrochem. Soc. 153 (2006) D123–D127.
[22] H.C. Liang, X.Z. Li, J. Hazard. Mater. 162 (2009) 1415–1422.

[23] S.P. Albu, A. Ghicov, S. Aldabergenova, P. Drechsel, D. LeClere, G.E. Thompson, J.M. Macak, P. Schmuki, Adv. Mater. 20 (2008) 4135.
[24] Y.C. Zhang, J. Li, H.Y. Xu, Appl. Catal. B Environ. 123 (2012) 18–26.
[25] Q.Y. Wang, X.C. Yang, D. Liu, L.N. Chi, J.W. Hou, Electrochim. Acta 83 (2012) 140–145.
[26] G.M. Guo, B.B. Yu, P. Yu, X. Chen, Talanta 79 (2009) 570–575.
[27] X.J. Xu, X.S. Fang, T.Y. Zhai, H.B. Zeng, B.D. Liu, X.Y. Hu, Y. Bando, D. Golberg, Small 7 (2011) 445–449.
[28] T.C. Zhang, X.Y. Hu, M. Fang, L.D. Zhang, Z.M. Wang, CrystEngComm 14 (2012) 7656–7661.
[29] G. Zhang, H. Huang, Y. Zhang, H.L.W. Chan, L. Zhou, Electrochem. Commun. 9 (2007) 2854–2858.
[30] D.A. Wang, Y. Liu, C.W. Wang, F. Zhou, W.M. Liu, ACS Nano 3 (2009) 1249–1257.
[31] Z. Grzesik, T. Bak, J. Nowotny, B. Henry, Adv. Appl. Ceram. 106 (2007) 77–81.
[32] X.Y. Hu, T. Zhang, Z. Jin, S.Z. Huang, M. Fang, Y.C. Wu, L. Zhang, Cryst. Growth Des. 9 (2009) 2324–2328.
[33] X.M. Sun, Y.D. Li, Chem. Eur. J. 9 (2003) 2229–2238.
[34] S. Tanaka, H. Tobimatsu, Y. Maruyama, T. Tanaki, G. Jerkiewicz, ACS Appl. Mater. Int. 1 (2009) 2312–2319.
[35] J.Q. Huang, Y.G. Cao, M.L. Wang, C.G. Huang, Z.H. Deng, H. Tong, Z.G. Liu, J. Phys. Chem. C 114 (2010) 14748–14754.
[36] Z. Jin, G.T. Fei, X.L. Cao, X.W. Wang, J. Nanosci. Nanotechnol. 10 (2010) 5471–5474.
[37] K.S.W. Sing, D.H. Everett, R.A.W. Haul, L. Moscou, R.A. Pierotti, J. Rouquerol, T. Siemieniewska, Pure Appl. Chem. 57 (1985) (1984) 603–619.
[38] H.X. Li, Z.F. Bian, J. Zhu, D.Q. Zhang, G.S. Li, Y.N. Huo, H. Li, Y.F. Lu, J. Am. Chem. Soc. 129 (2007) 8406.
[39] Y. Wang, Y. Wang, Y.L. Meng, H.M. Ding, Y.K. Shan, X. Zhao, X.Z. Tang, J. Phys. Chem. C 112 (2008) 6620–6626.
[40] H.Q. An, B.L. Zhu, J.X. Li, J. Zhou, S.R. Wang, S.M. Zhang, S.H. Wu, W.P. Huang, J. Phys. Chem. C 112 (2008) 18772–18775.